Structure of aquaporin-0 arrays in sphingomyelin/cholesterol membranes and implications for lipid rafts

Po-Lin Chiu[1,2] and Thomas Walz[1,3,*,#]

[1] Department of Cell Biology, Harvard Medical School, Boston, MA 02467, USA

[2] Current address: School of Molecular Sciences, Biodesign Center for Applied Structural Discovery, Arizona State University, Tempe, AZ 85287, USA

[3] Current address: Laboratory of Molecular Electron Microscopy, The Rockefeller University, New York, NY 10065, USA; Biogen, Cambridge, MA 02142, USA

[*] For correspondence: twalz@rockefeller.edu

[#] Lead Contact

Abstract

The tetrameric water channel aquaporin-0 (AQP0) forms square arrays in lens membranes through an as yet unknown mechanism. Lens membranes are enriched in cholesterol and sphingomyelin, suggesting that these raft lipids may play a role in AQP0 array formation. We produced two-dimensional crystals of AQP0 in sphingomyelin membranes with low and high cholesterol content and determined their structures by electron crystallography. At the higher cholesterol concentration, cholesterol associates with AQP0 and shifts lipids in the cytoplasmic leaflet away from the bilayer center, increasing the hydrophobic thickness of the annular lipid shell. AQP0 tetramers may thus

cluster to mitigate the resulting hydrophobic mismatch. Moreover, neighboring AQP0 tetramers sandwich a cholesterol in the center of the membrane. Since each tetramer interacts with four such 'glue' cholesterols, avidity effects may stabilize larger arrays. The principles proposed to drive AQP0 array formation could also underlie protein clustering in lipid rafts.

Introduction

The organization of biological membranes has classically been described by the fluid-mosaic model (Singer & Nicolson, 1972), in which lipids function as a two-dimensional (2D) solvent that allows membrane proteins to freely and randomly diffuse within the membrane plane. This model has been updated by the view that proteins do not freely float in the lipid bilayer but are densely packed and often organized into functional modules that perform specific biological functions (Engelman, 2005; Nicolson, 2014). The clustering of membrane proteins, which increases the efficiency of cellular processes (Cebecauer et al., 2010; Garcia-Parajo et al., 2014), is promoted by an increase in local protein concentration (Anishkin & Kung, 2013; de Meyer et al., 2010; Lillemeier et al., 2006; Lundbaek et al., 2003; Merklinger et al., 2017; Vereb et al., 2000). It has been recognized, however, that lipids also play an important role in organizing membrane proteins, and the resulting specialized membrane domains are now commonly known as lipid microdomains or lipid rafts (Karnovsky et al., 1982; Lingwood & Simons, 2010; Simons & Ikonen, 1997; Simons & Toomre, 2000; Stier & Sackmann, 1973; Vereb et al., 2003). The plasma membrane is thus best viewed as a patchwork of lipid microdomains that form transient platforms for diverse cellular processes, such as signal transduction

(Bauer & Pelkmans, 2006; Groves & Kuriyan, 2010; Himanen et al., 2007; Mugler et al., 2013), immune actions (Janes et al., 1999; Sheets et al., 1999; Varshney et al., 2016), endocytosis (Lang et al., 2001; Rodal et al., 1999; Subtil et al., 1999), neurotransmitter signaling (Allen et al., 2007), and virus entry (Chazal & Gerlier, 2003; Doherty & McMahon, 2009).

Lipid microdomains are enriched in cholesterol (Barenholz, 2002; Korade & Kenworthy, 2008; Simons & Ikonen, 1997) and characterized by a lipid phase that is distinct from the surrounding membrane (Ahmed et al., 1997; Schroeder et al., 1991). Cholesterol has a planar four-aromatic ring structure with a short isooctyl alkyl chain and a small 3-β-hydroxyl head group that can form a hydrogen bond with a polar group (Figure 1–figure supplement 1A). Because the aliphatic groups linked to the ring system are asymmetrically distributed, cholesterol features a smooth (or α) face and a rough (or β) face (Figure 1–figure supplement 1A). It is an essential lipid in eukaryotic cell membranes, in which it makes up 40-90% of the lipids (Liscum & Munn, 1999; van Meer et al., 2008). Because of its distinct structure, it can modulate the physical properties of membranes, such as fluidity, lateral pressure, curvature, and bilayer thickness (Yeagle, 1985), by forming non-covalent interactions with lipid acyl chains, preferentially with saturated ones (Epand & Epand, 2004; Zheng et al., 2007). This entropic interaction limits the flexibility of the acyl chains and thus reduces the surface area occupied by the interacting lipids. As a result, the membrane transitions from a liquid-disordered to a liquid-ordered phase (de Meyer et al., 2010; Ghysels et al., 2019; Marsh, 2010; Seelig, 1977), which has been linked to the formation of lipid microdomains (Quinn & Wolf, 2009; Silvius, 2003).

Mammalian lens membranes have a distinct lipid composition and contain a high percentage of sphingomyelin – a lipid consisting of a phosphocholine head group, a sphingosine amino alcohol and a fatty acid (Figure 1–figure supplement 1B) – and cholesterol, lipids that are characteristic for lipid rafts (Simons & Ikonen, 1997; Zelenka, 1984). With a molar ratio of cholesterol to other phospholipids ranging from 2.02 to 2.52, the human lens core plasma membrane features the highest molar cholesterol content of all membranes found in human tissues (Fleschner & Cenedella, 1991; Zelenka, 1984). Aquaporin-0 (AQP0), a lens-specific water channel, is the most abundant membrane protein in lens membranes (over 60% of the total protein content) (Alcalá et al., 1975; Bloemendal et al., 1972), where it forms large 2D arrays (Gorin et al., 1984; Kistler & Bullivant, 1980; Zampighi et al., 1982).

The propensity of AQP0 to form 2D crystals was used to determine its structure by electron crystallography of *in vitro* assembled 2D crystals grown with the lipid dimyristoyl phosphatidylcholine (DMPC) (Gonen et al., 2005). Later, AQP0 2D crystals were grown with a variety of different lipids (Hite et al., 2015; Hite et al., 2010). All these crystals had the same lattice constants, which were identical to those of AQP0 arrays in native lens membranes (Buzhynskyy et al., 2007). Thus, *in vitro* grown 2D crystals recapitulate the organization of AQP0 tetramers in 2D arrays in the native lens membrane. Interestingly, however, high-resolution electron crystallographic studies, which also resolved the annular lipids (Gonen et al., 2005; Hite et al., 2010), showed that AQP0 tetramers in the 2D crystals are separated by a layer of lipids and form essentially no direct protein–protein interactions. As the crystal contacts are almost exclusively

mediated by lipids, it is surprising that AQP0 2D crystals could be obtained with almost every lipid tested.

In vitro, AQP0 can be induced to form 2D crystals by choosing a very specific lipid-to-protein ratio (LPR) for reconstitution, which provides just enough lipids to form the single layer seen between adjacent AQP0 tetramers. This *in-vitro* approach does not explain, however, why AQP0 tetramers form 2D arrays in native lens membranes, which contain an excess of lipids as well as other membrane proteins. Since lipids mediate the interactions in AQP0 2D arrays, it is likely that specific lipids play a role in the assembly of AQP0 2D arrays in the native lens membrane. As AQP0-containing lens membrane junctions are greatly enriched in cholesterol and sphingomyelin (Fleschner & Cenedella, 1991), lipids that play a key role in raft formation (Brown & London, 2000), these lipids were prime candidates to drive AQP0 array formation. To gain structural insights into how cholesterol and/or sphingomyelin may induce AQP0 to form 2D crystals *in vivo* and potentially to obtain a more general understanding of how these lipids can establish lipid microdomains, we determined structures of AQP0 in membranes formed by mixtures of cholesterol and sphingomyelin.

Results

AQP0 forms 2D crystals with all tested cholesterol/sphingomyelin mixtures

Purified AQP0 was reconstituted with mixtures of sphingomyelin and cholesterol at molar ratios of 1:0, 3:1, 2:1, 1:1, 1:2, 1:4 and 0:1 (Figure 1A–E). Every lipid mixture yielded membranes, which had a sheet-like morphology at sphingomyelin:cholesterol ratios of up to 1:2 and formed vesicles at higher cholesterol percentages. In every case,

power spectra of images taken of trehalose-embedded samples showed diffraction spots consistent with typical 2D arrays of AQP0 (data not shown).

Notably, even reconstitution of AQP0 with pure cholesterol yielded vesicles, which displayed a tendency to stack (Figure 1E). Cholesterol on its own does not form bilayers under physiological conditions and requires a molecule of complementary shape to do so (Kumar, 1991; Raguz et al., 2011). AQP0 appears to fulfill this requirement as it does form membranes with cholesterol. However, reconstitution of AQP0 with cholesterol only yielded membranes within a narrow LPR range, from 0.2 to 0.4. At higher or lower LPRs, only protein aggregates and no membranes were observed.

Fourier transforms of cryo-EM images of trehalose-embedded AQP0 2D crystals formed with cholesterol at an LPR of 0.4 showed clear reflections (Figure 1–figure supplement 2), establishing that the crystals have the same lattice constants as all other AQP0 2D crystals analyzed to date (a = 65.5 Å, b = 65.5 Å, and γ = 90°). Phase comparisons of the reflections showed that the crystals have p422 plane symmetry (Table 1) and thus have to be double-layered. Merging of 15 images yielded a projection map at 3.2-Å resolution (Figure 1F and Table 2). Although the crystals were not of sufficient quality to determine a high-resolution three-dimensional (3D) density map, the 2D projection map shows that AQP0 tetramers in a pure cholesterol membrane are organized in the same way as in membranes formed with all other lipids analyzed to date.

Structure determination of AQP0$_{2SM:1Chol}$

Fourier transforms of images of trehalose-embedded AQP0 crystals obtained with sphingomyelin/cholesterol mixtures showed reflections to a resolution of about 2 Å (Chiu

et al., 2015). We focused first on AQP0 2D crystals obtained with a sphingomyelin/cholesterol mixture at a molar ratio of 2:1, from here on referred to as $AQP0_{2SM:1Chol}$. We collected electron diffraction patterns of these crystals at different tilt angles under low-dose conditions. While diffraction patterns recorded from untilted crystals showed reflections to a resolution of 2 Å (Figure 2A), reflections in diffraction patterns from highly tilted crystals were not visible beyond a resolution of 2.5 Å (Figure 2–figure supplement 1A).

After merging 214 diffraction patterns from crystals tilted up to ~72º and phasing the intensity dataset by molecular replacement, we were able to calculate a 3D density map at 2.5-Å resolution (Figure 2B), which made it possible to model the AQP0 structure. To build the sphingomyelin molecules, we initially only modeled the head groups and 10 carbon atoms for each of the two acyl chains. If the $2F_o$-F_c map after crystallographic refinement showed additional density, we extended the acyl chains, and this cycle was iterated. To avoid over-fitting, after each iteration, we assessed the values for R_{work}, R_{free} and their difference, as well as the consistency of the calculated $2F_o$-F_c map with the composite omit map. The final model includes seven sphingomyelin molecules, SM1 to SM7, with acyl chains ranging from 11 to 16 carbon atoms in length (Figure 3A). The one density in the map that was consistent with the characteristic four-ring structure of cholesterol was modeled as Chol1 (Figure 3A). The density in the center of four adjacent AQP0 tetramers around the four-fold symmetry axis was poorly resolved and could not be modeled (Figure 3–figure supplement 1B). The statistics for electron crystallographic data collection, model building, refinement and validation of $AQP0_{2SM:1Chol}$ are summarized in Table 3.

The structure of $AQP0_{2SM:1Chol}$ shows an AQP0 array with a low cholesterol content

AQP0 in the 2:1 sphingomyelin/cholesterol membrane adopts the same conformation as it does in a DMPC bilayer, $AQP0_{DMPC}$ (Gonen et al., 2005), and in an *E. coli* polar lipid extract (EPL) bilayer, $AQP0_{EPL}$ (Hite et al., 2010), with root mean square deviation (RMSD) between the Cα atoms of 0.271 Å and 0.264 Å, respectively (Figure 3–figure supplement 2A–B). The densities of the side chains along the water permeation pathway were clearly resolved as were the water molecules (Figure 2B). The water pathway through the AQP0 subunits showed density for four water molecules, at positions similar to those seen in previous electron crystallographic AQP0 structures (Gonen et al., 2004; Hite et al., 2010).

Comparison of the lipid bilayer in the $AQP0_{2SM:1Chol}$ structure (Figure 3A) with those in the $AQP0_{DMPC}$ and $AQP0_{EPL}$ structures (Figure 3B–C) shows that the seven sphingomyelin molecules assume similar positions as the DMPC and EPL lipids, further strengthening the earlier conclusion that annular lipids are not randomly distributed around a membrane protein but assume preferred positions (Hite et al., 2010). The density for sphingomyelin SM3 is well defined. The carbonyl oxygen of its head group is hydrogen-bonded with the tyrosyl side chain of Tyr105 and the amide oxygen of the guanidinium side chain of Arg196 (Figure 3–figure supplement 3A). However, the head groups of the remaining sphingomyelin lipids do not form specific interactions with AQP0, as reported for the DMPC and EPL head groups in the previous $AQP0_{DMPC}$ and $AQP0_{EPL}$ structures. Also, as observed in those structures, the sphingomyelin acyl chains follow grooves on the surface of AQP0.

The only cholesterol molecule, Chol1, resolved in the $AQP0_{2SM:1Chol}$ structure is located in the extracellular leaflet (Figure 3A). The tetracyclic ring of Chol1 makes π-stacking interactions with AQP0 residues His201 and Trp205, and its alkyl tail makes van der Waals interactions with residues Ile87 and Val90 (Figure 3–figure supplement 3B). Chol1 also interacts extensively with the adjacent sphingolipid in the extracellular leaflet, SM2, the acyl chains of which assume an all *anti*-dihedral conformation, increasing their conformational order (Figure 3–figure supplement 3B).

While Chol1 may increase the conformational order of adjacent SM2, this effect is unlikely to induce AQP0 to form an array. Similarly, the location of Chol1 with respect to adjacent AQP0 tetramers (Figure 3–figure supplement 1B) does not provide any clues as to how it could affect array formation *in situ*. We therefore decided to analyze the structure of AQP0 in a membrane that has a higher cholesterol content.

Structure determination of $AQP0_{1SM:2Chol}$

Lens membranes contain more cholesterol than is represented by the $AQP0_{2SM:1Chol}$ structure. Therefore, we determined the structure of AQP0 2D crystals that were grown at a molar sphingomyelin:cholesterol ratio of 1:2, which is close to the lipid composition of human lens core membranes (Fleschner & Cenedella, 1991; Zelenka, 1984). These crystals were even better ordered, and electron diffraction patterns of untilted specimens showed reflections to a resolution better than 1.6 Å (Figure 2C). Diffraction patterns of 2D crystals tilted to 60° showed reflections to a resolution of ~2.5 Å (Figure 2–figure supplement 1B). We used the same data collection and processing scheme for $AQP0_{2SM:1Chol}$ to obtain a density map for $AQP0_{1SM:2Chol}$ at 2.5 Å resolution (Figure 2D).

The density map allowed us to model AQP0, five sphingomyelin molecules, SM2, SM3, SM5, SM6 and SM7 (numbers corresponding to the sphingomyelin molecules in $AQP0_{2SM:1Chol}$) as well as four cholesterols (Figure 4A). As with the $AQP0_{1SM:2Chol}$ structure, it was not possible to model lipids in the area near the four-fold axis, where four AQP0 tetramers come together (Figure 3–figure supplement 1D). The statistics for the $AQP0_{1SM:2Chol}$ structure are summarized in Table 3.

The structure of $AQP0_{1SM:2Chol}$ shows an AQP0 array with a high cholesterol content

Superimposition of the $AQP0_{1SM:2Chol}$ structure with the $AQP0_{2SM:1Chol}$, $AQP0_{DMPC}$ and $AQP0_{EPL}$ structures yielded RMSD values between the Cα atoms of 0.431 Å, 0.390 Å and 0.362 Å (Figure 3–figure supplement 2C–E), again showing that the lipid environment has no detectable effect on the conformation of AQP0. Also, the water pathway in $AQP0_{1SM:2Chol}$ showed the same densities representing water molecules as observed in the $AQP0_{2SM:1Chol}$ structure. Hence, the AQP0 structure is essentially identical in the two analyzed sphingomyelin/cholesterol bilayers.

In the $AQP0_{2SM:1Chol}$ structure, an AQP0 subunit is surrounded by seven sphingomyelin molecules, but in the $AQP0_{1SM:2Chol}$ structure, due to the higher cholesterol content, two of the sphingomyelins in the extracellular leaflet, SM1 and SM4, have been replaced by cholesterols (Figure 4A–B). Of the two sphingomyelins remaining in the extracellular leaflet, the conformation of SM3 is virtually identical to that in the $AQP0_{2SM:1Chol}$ structure (Figure 4C). The other sphingomyelin in the extracellular leaflet, SM2, as well as the three sphingomyelins in the cytoplasmic leaflets, SM5 – SM7, all occupy similar positions as their counterparts in the $AQP0_{2SM:1Chol}$ structure, but adopt

different conformations. In particular, SM2 and SM6 adapt their conformation to accommodate the additional cholesterol molecules. With the exception of SM3, the head group of which is stabilized by identical interactions with AQP0 in $AQP0_{2SM:1Chol}$ and $AQP0_{1SM:2Chol}$, the head groups of all other corresponding sphingomyelins are different in the two structures (Figure 4C), corroborating the general lack of specific lipid–protein interactions in the head-group region.

The four cholesterol molecules in the $AQP0_{1SM:2Chol}$ structure show an interesting distribution. Overlaying the two bilayers shows that Chol1 in $AQP0_{1SM:2Chol}$ almost perfectly overlaps with Chol1 in $AQP0_{2SM:1Chol}$ (Figure 4C), and Chol1 interacts with AQP0 in the same way in the two structures, strengthening the notion that this is the preferred location for cholesterol to interact with AQP0. In the $AQP0_{2SM:1Chol}$ structure, Chol1 also interacts extensively with the adjacent sphingolipids, but some of these interactions are absent in the $AQP0_{1SM:2Chol}$ structure, due to the presence of the additional Chol2 (Figure 4A). The interaction with extracellular sphingomyelin SM1 in $AQP0_{2SM:1Chol}$ is replaced by an interaction with an acyl chain from cytoplasmic sphingomyelin SM5 (Figure 4C). Notably, however, despite their proximity, there do not seem to be any direct interactions between the two cholesterols (Figure 4–figure supplement 1A).

In addition to Chol1 and Chol2 in the extracellular leaflet, another cholesterol, Chol4, is located in the cytoplasmic leaflet (Figure 4A). Like Chol1 and Chol2, Chol4 interacts with AQP0 surface areas that feature aromatic residues (Figure 4D), in particular tryptophan and phenylalanine residues, which appear to make π-stacking

interactions with the cholesterol ring system (Burley & Petsko, 1985; McGaughey et al., 1998) (Figure 4–figure supplement 1).

Chol3 is the most unusual cholesterol molecule seen in the $AQP0_{1SM:2Chol}$ structure. While all other cholesterols are either within the extracellular or cytoplasmic leaflet, Chol3 is located almost in the middle of the bilayer, with its hydroxyl head group located in the middle of the extracellular leaflet (Figure 4A–figure supplement 3). The orientation of Chol3 is that of the other cholesterols in the extracellular leaflet, suggesting that it originated from that leaflet. There are three phenylalanine residues in the vicinity of Chol3, but these do not form π-stacking interactions with its ring system but are close to its acyl chain (Figure 4E).

Discussion

In this study, we determined two electron crystallographic structures of AQP0 in membranes formed by sphingomyelin and cholesterol. As these so-called raft lipids are the main constituents of lens membranes, they represent the natural environment of AQP0. The AQP0 crystals formed in sphingomyelin/cholesterol membranes have the same lattice constants as previous 2D crystals obtained with other lipids (Gonen et al., 2005; Hite et al., 2010) as well as the 2D arrays found in lens membranes (Buzhynskyy et al., 2007). The 2D crystals thus reflect the arrangement of AQP0 tetramers in native 2D arrays. As found previously, AQP0 has the same conformation in all analyzed 2D crystals irrespective of the lipid used for reconstitution.

Our structure of $AQP0_{2SM:1Chol}$ reveals seven sphingomyelins (Figure 3A), the same number of lipids also seen in structures of AQP0 in bilayers formed by DMPC

(Gonen et al., 2005) and EPL (Hite et al., 2010), and these are also located in almost identical positions (Figure 3B–C). The interaction of sphingomyelins with AQP0 thus seem to be governed by the same principles that were found for phosphoglycerolipids, namely that the acyl chains locate to grooves in the protein surface and that the lipid head groups make few if any interactions of with the protein (Hite et al., 2010). However, compared to the acyl chains in the EPL bilayer, those of the sphingomyelins appear to be straighter, which likely reflects the saturated nature of the sphingomyelin acyl chains (EPLs have ~55% unsaturated acyl chains (Mejía et al., 1999)). Despite this difference, the structure of the sphingomyelin bilayer is very similar to those of bilayers formed by phosphoglycerolipids, indicating that sphingomyelin by itself is unlikely the reason for AQP0 to form 2D arrays in lens membranes.

Cholesterol has a higher affinity for sphingomyelin than for phosphoglycerolipids (Niu & Litman, 2002), because the mostly saturated acyl chains of sphingomyelin can better accommodate the planar ring system of cholesterol (Epand & Epand, 2004; Zheng et al., 2007) and because the sphingomyelin backbone has two hydrogen-bond donor groups, an amide and a hydroxyl group, that make hydrogen bonding to cholesterol more effective (Róg & Pasenkiewicz-Gierula, 2006). Furthermore, the interaction of the sphingomyelin amide group with the hydroxyl group of cholesterol orients the smooth (α) face of the cholesterol towards sphingomyelin, leaving only the rough (β) face to interact with membrane proteins (Fantini & Barrantes, 2013). In the context of AQP0 2D arrays, however, these interactions do not appear to occur. While Chol1 does interact with sphingomyelin acyl chains in both structures, the additional cholesterols in the $AQP0_{1SM:2Chol}$ structure seem to have little interactions with sphingomyelin acyl chains

and instead seem to substitute for some of the sphingomyelin acyl chains seen in the $AQP0_{2SM:1Chol}$ structure (Figure 4A and C). We also do not observe interactions between the hydroxyl head group of any cholesterols with an amide group of the sphingomyelins. While we cannot rule out that specific sphingomyelin–cholesterol interactions occur in the membrane area enclosed by four AQP0 tetramers (where we were unable to build models for the lipids due to the four-fold symmetry axis), our structures suggest that specific sphingomyelin–cholesterol interactions do not play a critical role in AQP0 array formation in the lens membrane.

Cholesterol increases the order of lipid acyl chains (de Meyer & Smit, 2009; Lafleur et al., 1990), and the resulting phase transition is thought to contribute to the segregation of cholesterol-enriched membrane areas (Pandit et al., 2007). A potential mechanism by which cholesterol could induce AQP0 array formation could thus be that cholesterol bound to AQP0 would order the surrounding lipids, leading to a phase transition that leads to an initial segregation and crystallization of the AQP0/cholesterol/sphingomyelin units in the membrane.

In an attempt to assess this possibility, we looked at the *B*-factors of the acyl chains, which are affected, among other factors, by the mobility of the atoms. Comparison of corresponding acyl chains showed that the *B*-factors of the acyl chains in the $AQP0_{1SM:2Chol}$ structure tend to be slightly lower than those of the acyl chains in the $AQP0_{2SM:1Chol}$ structure (Figure 4–figure supplement 2), suggesting that the cholesterols could have an ordering effect on the sphingomyelin acyl chains. However, the *B*-factors of the acyl chains in the $AQP0_{EPL}$ structure, which contain double bonds and are not constrained by cholesterol and should thus be much less ordered, are similar to those of

the acyl chains in the $AQP0_{2SM:1Chol}$ structure. A likely explanation is that acyl chains, including unsaturated ones, preferentially fill in grooves in the protein surface (Hite et al., 2010), which should already substantially constrain their mobility. Therefore, cholesterol bound to the protein surface may not add much additional constraints to their already restricted mobility. Cholesterol-induced phase separation thus does not seem to be a likely cause for AQP0 array formation.

The hydrophobic thickness is an important characteristic of a lipid bilayer, which depends on the length and saturation of the acyl chains of the lipids forming the bilayer. Mismatch of the hydrophobic thickness between a membrane protein and the lipid bilayer is thought to be one mechanism by which membrane proteins can cluster in a membrane (Hanulová & Weiss, 2012; Schmidt et al., 2008). One factor that affects the hydrophobic thickness of a membrane is its cholesterol content, which is related to the ordering effect of cholesterol on the lipid acyl chains (de Meyer & Smit, 2009; Lafleur et al., 1990). Change in cholesterol-induced hydrophobic thickness may thus be another potential force that drives the formation of AQP0 arrays in the lens membrane.

To assess the influence of cholesterol content on the hydrophobic thickness of the membrane, we measured the average distance between the phosphor atoms of the phosphodiester groups and the nitrogen atoms of the amide groups of the sphingomyelins in the two leaflets (Figure 1–figure supplement 1), which were 36.8 Å and 31.3 Å, respectively, for the $AQP0_{1SM:2Chol}$ bilayer (Figure 4A) and 33.9 Å and 27.1 Å, respectively, for the $AQP0_{2SM:1Chol}$ bilayer (Figure 4B). As both distances are larger for the bilayer with the higher cholesterol content, by ~3 Å for the phosphodiester groups

and ~4 Å for the amide groups, it appears that a higher cholesterol content indeed increases the hydrophobic thickness of the bilayer formed by the annular sphingomyelins.

In cells, sphingomyelin is predominantly found in the extracellular leaflet of the plasma membrane (Devaux, 1991), so that sphingomyelins seen in the extracellular leaflet in our two structures likely represent true positions of sphingomyelin in native AQP0 2D arrays. The two sphingomyelins in the extracellular leaflet that are seen in both sphingomyelin/cholesterol membranes are in exactly the same position (Figure 4C), establishing that the extracellular leaflet does not change its position relative to AQP0 upon thickening of the membrane with increasing cholesterol content. Sphingomyelin SM3 may be responsible for the fixed position of the extracellular leaflet. In all structures of AQP0 in different lipid bilayers, the lipid at the position equivalent to that of SM3 always has the best-defined density and the lowest *B*-factors (including for the acyl chains; Figure 4–figure supplement 2). The lipid at this position is always the only one whose head group makes interactions with AQP0. It is thus possible that the lipid at this position defines and locks in the position of the extracellular leaflet with respect to AQP0. As a result, the extracellular leaflet does not play a role in defining the thickness of the membrane.

The increase in hydrophobic thickness with higher cholesterol content is the result of the three sphingomyelins in the cytoplasmic leaflet moving further out from the bilayer center, which they do even though this leaflet contains only a single cholesterol (Figure 4C). Despite the caveat that our $AQP0_{1SM:2Chol}$ bilayer structure shows a lipid distribution opposite of the expected one (more sphingomyelin in the cytoplasmic leaflet and more cholesterol in the extracellular leaflet), the notion that an increase in hydrophobic

thickness is predominantly due to movements of lipids in the cytoplasmic leaflet is consistent with the observation that these lipids are usually more mobile, i.e., have higher *B*-factors in crystal structure than lipids in the extracellular leaflet (Belrhali et al., 1999). Comparison of the lipid arrangement in the cytoplasmic leaflet shows that Chol4 in the $AQP0_{1SM:2Chol}$ structure assumes the position of SM6 in the $AQP0_{2SM:1Chol}$ structure (Figure 4A–C). The new position of the displaced SM6 in the $AQP0_{1SM:2Chol}$ structure is further out from the bilayer center and potentially is the cause for similar outward movements of lipids SM5 and SM7, thus defining the new position of the cytoplasmic leaflet and increasing the hydrophobic thickness of the bilayer. Hence, a higher cholesterol concentration of the membrane does increase the hydrophobic thickness of the lipid bilayer formed by the annular lipids surrounding AQP0 tetramers, thus creating a hydrophobic mismatch with the remaining lipid bilayer, which, in turn, would drive AQP0 tetramers to cluster in the native lens membrane.

Both structures of AQP0 in sphingomyelin/cholesterol membranes show fewer cholesterols than should be present in the membranes with observed molar sphingomyelin:cholesterol ratios of 7:1 and 4:5 (instead of 2:1 and 1:2). The cholesterols that are not visible may either be stochastically distributed at positions predominantly occupied by sphingomyelin acyl chains or they may accumulate in the area where four AQP0 tetramers come together and where lipids cannot be modeled due to the four-fold symmetry axis (Figure 3–figure supplement 1B and D) or both. It is also possible that due to the low solubility of cholesterol, the lipid mixtures used for 2D crystallization contained less cholesterol than targeted. While we cannot be sure what the reason is for

the lower-than-anticipated number of cholesterols in our structures, it does not affect the conclusions that can be drawn from the structures.

The $AQP0_{2SM:1Chol}$ structure shows a single cholesterol, Chol1, in the extracellular leaflet (Figure 3A). This cholesterol is seen in an almost identical position in the $AQP0_{1SM:2Chol}$ structure (Figure 4A and C), in which it is, however, in close proximity to another cholesterol, Chol2. Remarkably, very similar positions and interactions of cholesterol with AQP0 have previously been described in a molecular dynamics (MD) simulation study of an AQP0 tetramer embedded in a cholesterol-containing DMPC bilayer (O'Connor & Klauda, 2011), and is further supported by the accompanying paper that used the presented $AQP0_{2SM:1Chol}$ and $AQP0_{1SM:2Chol}$ for further MD analyses (Orjuela et al., submitted). This agreement suggests that the observed position of Chol1, and maybe also Chol2, represent preferred interaction sites of cholesterol with AQP0. These sites seem to be independent of the composition of the lipid bilayer, as they are identical in a sphingomyelin and a DMPC bilayer.

In the $AQP0_{1SM:2Chol}$ structure, there is also a cholesterol in the cytoplasmic leaflet. Cholesterol is thought to be distributed equally between the two bilayer leaflets or potentially to localize predominantly to the cytoplasmic leaflet (Buwaneka et al., 2021; Giang & Schick, 2016). It is thus somewhat surprising to see more cholesterol in the extracellular leaflet than in the cytoplasmic leaflet. However, since the molar cholesterol:phospholipid ratio of lens membranes is very high, 2.2 to 9.2 (Borchman et al., 1989) and since there are few positions left in the extracellular leaflet that could be occupied by cholesterol, it is reasonable that higher cholesterol concentrations in the membrane would lead to a more equal distribution of cholesterol between the two

leaflets. For this reason, and because Chol4 in the cytoplasmic leaflet interacts with AQP0 in the same fashion as the two cholesterols in the extracellular leaflet, Chol1 and Chol2, namely with hydrophobic residues as well as involving π-stacking interactions between their ring system and aromatic residues of AQP0, all these observed cholesterol positions are likely to be found in native AQP0 arrays. The cholesterols do not bind to AQP0 through consensus cholesterol-binding sites known as the Cholesterol Recognition/interaction Aminoacid Consensus sequence (CRAC domain; -L/V-$(X)_{1-5}$-Y-$(X)_{1-5}$-R/K-) (Li & Papadopoulos, 1998) or the inverted CRAC domain, CARC (Baier et al., 2011). Cholesterol can also bind to membrane proteins in a fashion that does not involve a CRAC or CARC domain, as seen for example for the influenza M2 protein (Elkins et al., 2018; Elkins et al., 2017) and α-synuclein (Fantini et al., 2011). Emerging cryo-EM structures of G protein-coupled receptors (GPCRs) also do not show a consensus motif for their interaction with cholesterol (Sarkar & Chattopadhyay, 2020; Taghon et al., 2021). Furthermore, the cholesterols interact with AQP0 through their smooth α face (Figure 4–figure supplement 1), which is not engaged in interactions with sphingomyelin as previously thought (Fantini & Barrantes, 2013), thus differing from the predominant interaction of cholesterols with GPCRs, the G-protein-gated inwardly rectifying potassium-2 (GIRK2) channel, and the Na^+, K^+-ATPase, which occur predominantly through the rough β face of cholesterol (Gimpl, 2016; Mathiharan et al., 2021; Shinoda et al., 2009). However, there are other cases in which cholesterol interacts with membrane proteins through its α face, such as seen for the Niemann-Pick C1-like 1 protein (Huang et al., 2020). Likely the residues on the protein surface determine whether a protein interacts with cholesterol through its α or β face. The smooth α face interacts

with aromatic side chains through π-stacking (Nishio et al., 1995), whereas the β face appears to interact with hydrophobic side chains, such as leucine, valine, or isoleucine (Fantini et al., 2011).

Chol3 is the most unusual lipid in our structure, because it is located in the middle of the lipid bilayer, because it interacts with AQP0 differently from the other three cholesterols, and because it is sandwiched between two neighboring AQP tetramers. Binding sites for cholesterol in the middle of the membrane have also been described for GPCRs, and these sites have been named "deep binding sites" (Genheden et al., 2017). A docking investigation with known membrane protein structures for cholesterol-binding sites revealed deep binding sites not only in GPCRs but also in ion channels and transporters (Lee, 2018). Unlike any other cholesterol in our structures, Chol3 interacts directly with two AQP0 subunits that are part of different tetramers. This interaction is different from the cholesterol-induced dimerization of GPCRs as these are mediated by interactions between two or more cholesterol molecules rather than one cholesterol directly interacting with two GPCRs (Gimpl, 2016; Hanson et al., 2008). The two adjacent AQP0 tetramers form a pocket that is ~8.5 Å wide at the position of the ring system and ~2.5 Å at the position of the acyl chain (Figure 4E). The interaction surface on the AQP0 subunit interacting with the smooth face of Chol3 encompasses 373 $Å^2$ and is formed by residues Ser106, Val103, Ala102, Ala99, and Leu21, which line the ring system, and three phenylalanine residues, Phe17, Phe18 and Phe14, which surround the acyl chain. The interaction surface on the AQP0 subunit interacting with the rough face of Chol3 is 344 $Å^2$ and is predominantly formed by residues Ile132, Ile135, Phe136, Ile210, Leu214, and Leu217 (Figure 4E). Leucine and isoleucine residues have also been

found to mediate the interaction of many GPCRs with the rough β face of cholesterol (Gimpl, 2016). The hydroxyl head group of Chol3 interacts with a water molecule that may be stabilized through an interaction with Ser126 (Figure 4E). Because of its intricate interactions with two AQP0 subunits, Chol3 can likely function as a glue that can keep two tetramers together. This structural characteristic may be the reason why AQP0 can form 2D arrays in pure cholesterol membranes (Figure 1E and 1F). The accompanying manuscript that presents MD studies based on our structures shows that adjacent AQP0 tetramers does stabilize the sandwiched cholesterol in the middle of the membrane and that this glue cholesterol does indeed strengthen the interaction between the two associated AQP0 tetramers (Orjuela et al., submitted).

Our structures of AQP0 arrays in sphingomyelin bilayers with low and high cholesterol content and the results from the MD simulations (Orjuela et al., submitted) allow us to propose a model for cholesterol-induced array formation (Figure 5). In a lipid bilayer with a low cholesterol concentration, cholesterol may interact with AQP0 predominantly through the most specific cholesterol-binding site, the one occupied by Chol1, but this interaction would be transient and would not have a meaningful effect on the organization of the surrounding lipid molecules (sphingomyelin in our $AQP0_{2SM:1Chol}$ structure) (Figure 5A). An increase in cholesterol concentration will cause more cholesterols in the extracellular leaflet to bind to AQP0. In addition, cholesterol will also enrich in the cytoplasmic leaflet and associate with AQP0. This interaction will shift the annular lipids in this leaflet further away from the membrane center and create a hydrophobic mismatch between the shell of annular lipids and the surrounding lipid bilayer (Figure 5B). Driven by the force to minimize membrane tension induced by

hydrophobic mismatch, AQP0 tetramers will cluster. Cholesterols in between the tetramers can diffuse deeper into the membrane and associate with deep binding sites on AQP0, thus stabilizing the interaction between adjacent tetramers (Figure 5C). Alternatively, it may also be possible that cholesterol first interacts with a deep binding site on one AQP0 but is only stabilized as the second AQP0 traps it in position. As each AQP0 tetramer has four deep cholesterol-binding sites, the avidity effect would result in the formation and stabilization of large 2D arrays as those seen in native lens membranes (Figure 5D).

This model is specific for the formation of AQP0 arrays in lens membranes, but similar principles may underlie the organization of lipid rafts. AQP0 may be special in that it forms tetramers and thus has four deep cholesterol-binding sites, so that the avidity effect allows it to form much larger domains than seen for typical lipid rafts (Simons & Ikonen, 1997; Zelenka, 1984). In addition, it is presumably not common that the same protein has surfaces that can interact with both the smooth α and the rough β face of cholesterol. However, cholesterol would have the potential to mediate the association of any protein with an α face-interacting surface with any other protein that features a β face-interacting surface. Thus, while hydrophobic mismatch and phase separation may be driving forces that bring proteins into close proximity, cholesterol may be the actual glue that increases the time they remain associated.

Materials and methods

Purification of AQP0

AQP0 was purified as described in Gonen et al. (2004). Briefly, dissected cores of sheep lenses (Wolverine Packing Company, Detroit, MI) were homogenized, and isolated membranes were sequentially washed with 10 mM Tris-HCl, pH 8.0, 4 M urea, and 20 mM NaOH, and then solubilized with 4% n-octyl-β-D-glucopyranoside (OG; Anatrace). Solubilized AQP0 was purified using anion-exchange (MonoQ; GE Healthcare) and size-exclusion (Superose-6; GE Healthcare) chromatography.

2D crystallization of AQP0

Purified AQP0 in 1.2% OG, 10 mM Tris-HCl (pH 8.0), and 100 mM NaCl was mixed at a lipid-to-protein ratio (LPR) (w/w) of 0.2 with different mixtures of OG-solubilized sphingomyelin (N-palmitoyl-D-erythro-sphingosylphosphorylcholine) (Avanti) and cholesterol (Avanti). The mixtures were placed into dialysis buttons, and the detergent was removed by dialysis at 37°C against 10 mM MES (pH 6.0), 300 mM NaCl, 30 mM $MgCl_2$, and 0.05% NaN_3 for one week with daily buffer exchanges. The 2D crystal samples were prepared by negative staining with uranyl formate and assessed on a Philips CM10 electron microscope.

Imaging and image processing of AQP0 2D crystals grown with pure cholesterol

$AQP0_{Chol}$ 2D crystals were prepared on molybdenum grids using the carbon sandwich method (Gyobu et al., 2004) and a trehalose concentration ranging from 3% to 5% (w/v). After blotting away excess trehalose solution with a filter paper, grids were quick-frozen in liquid nitrogen and transferred onto a cryo-specimen stage for EM data collection.

Data of untilted 2D crystals were collected with a Polara electron microscope (FEI Company, Hillsboro, OR) operated at an acceleration voltage of 300 kV and equipped with a Gatan K2 Summit direct electron detector camera (Gatan, Pleasanton, CA), using low-dose procedures, a calibrated magnification of 50,926x, and a defocus ranging from -500 to -1500 nm. Dose-fractionated images were recorded in super-resolution mode at a counting rate of 8 counts/pixel/sec (8.33 counts/$Å^2$/sec). Frames were read out every 150 ms and 16 frames were collected, resulting in an exposure time of 2.4 seconds and a total dose of 20 $e^-/Å^2$. Motion-corrected sum images were generated using the program MotionCorr (Li et al., 2013).

Images of $AQP0_{Chol}$ were computationally unbent and corrected for the effects of the contrast transfer function using the 2dx software (Gipson, Zeng, Zhang, et al., 2007). The plane group symmetry of the projection map was analyzed with ALLSPACE (Table 1) (Valpuesta et al., 1994). Fifteen images were merged using 2dx_merge (Gipson, Zeng, & Stahlberg, 2007), resulting in a projection map at 3.2 Å resolution. The phase residuals are listed in Table 2.

Collection of electron diffraction data

2D crystals grown at molar sphingomyelin:cholesterol ratios of 1:2 and 2:1 were prepared by trehalose embedding as described above.

Electron diffraction patterns of AQP0 2D crystals were recorded with a Polara electron microscope (FEI Company, Hillsboro, OR) operated at an acceleration voltage of 300 kV and equipped with a 4k × 4k CCD camera (Gatan, Pleasanton, CA). The camera length was set to 1.9 m and a C2 aperture with a diameter of 30 μm was selected.

The selected target areas on the grids were exposed for 30 seconds, corresponding to a total electron dose of approximately 10 electrons/$Å^2$. Diffraction patterns were collected at tilt angles of 0°, 20°, 45°, 60°, 65°, and 70°, and details are provided in Table 3.

Diffraction data processing and model building

The graphical user interface of the IPLT diffraction processing software was used to index electron diffraction patterns (Schenk et al., 2013). Diffraction patterns that showed multiple 2D lattices were discarded. After subtracting the background resulting from inelastic scattering, the intensities of the reflections were extracted, integrated according to their 2D Miller indices, and then merged into reciprocal lattice lines as described before (Gonen et al., 2004). The reconstructed 3D lattice lines were then iteratively refined against the experimental data enforcing a *p*422 plane symmetry. The refined lattice lines were sampled along the z^* direction using the "truncate" program in the CCP4 software package (Winn et al., 2011), assuming a crystal thickness of 200 Å. The dataset was phased by molecular replacement in PHASER (version 2.1) (McCoy et al., 2007), using as search template the $AQP0_{DMPC}$ structure (PDB code: 2B6O) but without the loops and C-terminal domain of AQP0 and without the DMPC lipids. The density map obtained with data recorded from AQP0 2D crystals formed with a molar sphingomyelin:cholesterol ratio of 2:1 allowed building of AQP0 residues Ser6 to Pro225 as well as seven sphingomyelins and one cholesterol. For the density map obtained with AQP0 crystals formed with a sphingomyelin:cholesterol ratio of 1:2, AQP0 could also be built from Ser6 to Pro225, and five sphingomyelin and four cholesterol molecules could be built. Models were built in Coot (version 0.8.2) (Emsley & Cowtan, 2004), and the

topologies and geometry restraint parameters for cholesterol and sphingomyelin were generated using the eLBOW program (Moriarty et al., 2009). The model was refined in CNS (version 1.3) (Brünger et al., 1998) and Phenix (version 1.20.1) (Adams et al., 2010). Refinement statistics are summarized in Table 3. Figures were generated with PyMOL (version 1.8) (The PyMOL Molecular Graphics System, Schrödinger, LLC) and UCSF Chimera (version 1.10) (Pettersen et al., 2004).

Data availability

Model coordinates with the electron diffraction data in this study were deposited in the Protein Data Bank (PDB) under accession numbers 8SJY ($AQP0_{1SM:2Chol}$) and 8SJX ($AQP0_{2SM:1Chol}$). All data are available in the wwPDB database or from authors upon request.

Acknowledgments

We thank Zongli Li and Andreas Schenk for support in data collection and processing. This work was supported by National Institutes of Health grant R01 EY015107.

Additional Information

Author Contributions

P.L.C. performed biochemistry, EM data collection and processing, and structure determination. T.W. guided the project. P.L.C. and T.W. prepared the manuscript.

Author ORCIDs

Po-Lin Chiu – 0000-0001-8608-7650

Thomas Walz – 0000-0003-2606-2835

Declaration of Interests

The authors declare no competing interests.

References

Adams, P. D., Afonine, P. V., Bunkóczi, G., Chen, V. B., Davis, I. W., Echols, N., Headd, J. J., Hung, L.-W., Kapral, G. J., Grosse-Kunstleve, R. W., McCoy, A. J., Moriarty, N. W., Oeffner, R., Read, R. J., Richardson, D. C., Richardson, J. S., Terwilliger, T. C., & Zwart, P. H. (2010). PHENIX: a comprehensive Python-based system for macromolecular structure solution. *Acta Crystallogr D Biol Crystallogr*, *66*(Pt 2), 213-221. https://doi.org/10.1107/S0907444909052925

Ahmed, S. N., Brown, D. A., & London, E. (1997). On the origin of sphingolipid/cholesterol-rich detergent-insoluble cell membranes: physiological concentrations of cholesterol and sphingolipid induce formation of a detergent-insoluble, liquid-ordered lipid phase in model membranes. *Biochemistry*, *36*(36), 10944-10953. https://doi.org/10.1021/bi971167g

Alcalá, J., Lieska, N., & Maisel, H. (1975). Protein composition of bovine lens cortical fiber cell membranes. *Exp Eye Res*, *21*(6), 581-595.

Allen, J. A., Halverson-Tamboli, R. A., & Rasenick, M. M. (2007). Lipid raft microdomains and neurotransmitter signalling. *Nat Rev Neurosci*, *8*(2), 128-140. https://doi.org/10.1038/nrn2059

Anishkin, A., & Kung, C. (2013). Stiffened lipid platforms at molecular force foci. *Proc Natl Acad Sci U S A*, *110*(13), 4886-4892. https://doi.org/10.1073/pnas.1302018110

Baier, C. J., Fantini, J., & Barrantes, F. J. (2011). Disclosure of cholesterol recognition motifs in transmembrane domains of the human nicotinic acetylcholine receptor. *Sci Rep*, *1*, 69. https://doi.org/10.1038/srep00069

Barenholz, Y. (2002). Cholesterol and other membrane active sterols: from membrane evolution to "rafts". *Prog Lipid Res*, *41*(1), 1-5.

Bauer, M., & Pelkmans, L. (2006). A new paradigm for membrane-organizing and -shaping scaffolds. *FEBS Lett*, *580*(23), 5559-5564. https://doi.org/10.1016/j.febslet.2006.08.077

Belrhali, H., Nollert, P., Royant, A., Menzel, C., Rosenbusch, J. P., Landau, E. M., & Pebay-Peyroula, E. (1999). Protein, lipid and water organization in bacteriorhodopsin crystals: a molecular view of the purple membrane at 1.9 A resolution. *Structure*, *7*(8), 909-917.

Bloemendal, H., Zweers, A., Vermorken, F., Dunia, I., & Benedetti, E. L. (1972). The plasma membranes of eye lens fibres. Biochemical and structural characterization. *Cell Differ*, *1*(2), 91-106.

Borchman, D., Delamere, N. A., McCauley, L. A., & Paterson, C. A. (1989). Studies on the distribution of cholesterol, phospholipid, and protein in the human and bovine lens. *Lens Eye Toxic Res*, *6*(4), 703-724.

Brown, D. A., & London, E. (2000). Structure and function of sphingolipid- and cholesterol-rich membrane rafts. *J Biol Chem*, *275*(23), 17221-17224. https://doi.org/10.1074/jbc.R000005200

Brünger, A. T., Adams, P. D., Clore, G. M., DeLano, W. L., Gros, P., Grosse-Kunstleve, R. W., Jiang, J. S., Kuszewski, J., Nilges, M., Pannu, N. S., Read, R. J., Rice, L. M., Simonson, T., & Warren, G. L. (1998). Crystallography & NMR system: A new software suite for macromolecular structure determination. *Acta Crystallogr D Biol Crystallogr*, *54*(Pt 5), 905-921.

Burley, S. K., & Petsko, G. A. (1985). Aromatic-aromatic interaction: a mechanism of protein structure stabilization. *Science*, *229*(4708), 23-28.

Buwaneka, P., Ralko, A., Liu, S. L., & Cho, W. (2021). Evaluation of the available cholesterol concentration in the inner leaflet of the plasma membrane of mammalian cells. *J Lipid Res*, *62*, 100084. https://doi.org/10.1016/j.jlr.2021.100084

Buzhynskyy, N., Hite, R. K., Walz, T., & Scheuring, S. (2007). The supramolecular architecture of junctional microdomains in native lens membranes. *EMBO Rep*, *8*(1), 51-55. https://doi.org/10.1038/sj.embor.7400858

Cebecauer, M., Spitaler, M., Sergé, A., & Magee, A. I. (2010). Signalling complexes and clusters: functional advantages and methodological hurdles. *J Cell Sci*, *123*(Pt 3), 309-320. https://doi.org/10.1242/jcs.061739

Chazal, N., & Gerlier, D. (2003). Virus entry, assembly, budding, and membrane rafts. *Microbiol Mol Biol Rev*, *67*(2), 226-237, table of contents.

Chiu, P.-L., Li, X., Li, Z., Beckett, B., Brilot, A. F., Grigorieff, N., Agard, D. A., Cheng, Y., & Walz, T. (2015). Evaluation of super-resolution performance of the K2 electron-counting camera using 2D crystals of aquaporin-0. *J Struct Bio*, *192*(2), 163-173. https://doi.org/10.1016/j.jsb.2015.08.015

de Meyer, F., & Smit, B. (2009). Effect of cholesterol on the structure of a phospholipid bilayer. *Proc Natl Acad Sci U S A*, *106*(10), 3654-3658. https://doi.org/10.1073/pnas.0809959106

de Meyer, F. J., Benjamini, A., Rodgers, J. M., Misteli, Y., & Smit, B. (2010). Molecular simulation of the DMPC-cholesterol phase diagram. *J Phys Chem B*, *114*(32), 10451-10461. https://doi.org/10.1021/jp103903s

Devaux, P. F. (1991). Static and dynamic lipid asymmetry in cell membranes. *Biochemistry*, *30*(5), 1163-1173.

Doherty, G. J., & McMahon, H. T. (2009). Mechanisms of endocytosis. *Annu Rev Biochem*, *78*, 857-902. https://doi.org/10.1146/annurev.biochem.78.081307.110540

Elkins, M. R., Sergeyev, I. V., & Hong, M. (2018). Determining Cholesterol Binding to Membrane Proteins by Cholesterol. *J Am Chem Soc*, *140*(45), 15437-15449. https://doi.org/10.1021/jacs.8b09658

Elkins, M. R., Williams, J. K., Gelenter, M. D., Dai, P., Kwon, B., Sergeyev, I. V., Pentelute, B. L., & Hong, M. (2017). Cholesterol-binding site of the influenza M2 protein in lipid bilayers from solid-state NMR. *Proc Natl Acad Sci U S A*, *114*(49), 12946-12951. https://doi.org/10.1073/pnas.1715127114

Emsley, P., & Cowtan, K. (2004). Coot: model-building tools for molecular graphics. *Acta Crystallogr D Biol Crystallogr*, *60*(Pt 12 Pt 1), 2126-2132. https://doi.org/10.1107/S0907444904019158

Engelman, D. M. (2005). Membranes are more mosaic than fluid. *Nature*, *438*(7068), 578-580. https://doi.org/10.1038/nature04394

Epand, R. M., & Epand, R. F. (2004). Non-raft forming sphingomyelin-cholesterol mixtures. *Chem Phys Lipids*, *132*(1), 37-46. https://doi.org/10.1016/j.chemphyslip.2004.09.012

Fantini, J., & Barrantes, F. J. (2013). How cholesterol interacts with membrane proteins: an exploration of cholesterol-binding sites including CRAC, CARC, and tilted domains. *Front Physiol*, *4*, 31. https://doi.org/10.3389/fphys.2013.00031

Fantini, J., Carlus, D., & Yahi, N. (2011). The fusogenic tilted peptide (67-78) of α-synuclein is a cholesterol binding domain. *Biochim Biophys Acta*, *1808*(10), 2343-2351. https://doi.org/10.1016/j.bbamem.2011.06.017

Fleschner, C. R., & Cenedella, R. J. (1991). Lipid composition of lens plasma membrane fractions enriched in fiber junctions. *J Lipid Res*, *32*(1), 45-53.

Garcia-Parajo, M. F., Cambi, A., Torreno-Pina, J. A., Thompson, N., & Jacobson, K. (2014). Nanoclustering as a dominant feature of plasma membrane organization. *J Cell Sci*, *127*(Pt 23), 4995-5005. https://doi.org/10.1242/jcs.146340

Genheden, S., Essex, J. W., & Lee, A. G. (2017). G protein coupled receptor interactions with cholesterol deep in the membrane. *Biochim Biophys Acta*, *1859*(2), 268-281. https://doi.org/10.1016/j.bbamem.2016.12.001

Ghysels, A., Krämer, A., Venable, R. M., Teague, W. E., Lyman, E., Gawrisch, K., & Pastor, R. W. (2019). Permeability of membranes in the liquid ordered and liquid disordered phases. *Nat Commun*, *10*(1), 5616. https://doi.org/10.1038/s41467-019-13432-7

Giang, H., & Schick, M. (2016). On the puzzling distribution of cholesterol in the plasma membrane. *Chem Phys Lipids*, *199*, 35-38. https://doi.org/10.1016/j.chemphyslip.2015.12.002

Gimpl, G. (2016). Interaction of G protein coupled receptors and cholesterol. *Chem Phys Lipids*, *199*, 61-73. https://doi.org/10.1016/j.chemphyslip.2016.04.006

Gipson, B., Zeng, X., & Stahlberg, H. (2007). 2dx_merge: data management and merging for 2D crystal images. *J Struct Biol*, *160*(3), 375-384. https://doi.org/10.1016/j.jsb.2007.09.011

Gipson, B., Zeng, X., Zhang, Z. Y., & Stahlberg, H. (2007). 2dx--user-friendly image processing for 2D crystals. *J Struct Biol*, *157*(1), 64-72. https://doi.org/10.1016/j.jsb.2006.07.020

Gonen, T., Cheng, Y., Sliz, P., Hiroaki, Y., Fujiyoshi, Y., Harrison, S. C., & Walz, T. (2005). Lipid-protein interactions in double-layered two-dimensional AQP0 crystals. *Nature*, *438*(7068), 633-638. https://doi.org/10.1038/nature04321

Gonen, T., Sliz, P., Kistler, J., Cheng, Y., & Walz, T. (2004). Aquaporin-0 membrane junctions reveal the structure of a closed water pore. *Nature*, *429*(6988), 193-197. https://doi.org/10.1038/nature02503

Gorin, M. B., Yancey, S. B., Cline, J., Revel, J. P., & Horwitz, J. (1984). The major intrinsic protein (MIP) of the bovine lens fiber membrane: characterization and structure based on cDNA cloning. *Cell*, *39*(1), 49-59.

Groves, J. T., & Kuriyan, J. (2010). Molecular mechanisms in signal transduction at the membrane. *Nat Struct Mol Biol*, *17*(6), 659-665.

Gyobu, N., Tani, K., Hiroaki, Y., Kamegawa, A., Mitsuoka, K., & Fujiyoshi, Y. (2004). Improved specimen preparation for cryo-electron microscopy using a symmetric carbon sandwich technique. *J Struct Biol*, *146*(3), 325-333. https://doi.org/10.1016/j.jsb.2004.01.012

Hanson, M. A., Cherezov, V., Griffith, M. T., Roth, C. B., Jaakola, V. P., Chien, E. Y., Velasquez, J., Kuhn, P., & Stevens, R. C. (2008). A specific cholesterol binding site is established by the 2.8 A structure of the human beta2-adrenergic receptor. *Structure*, *16*(6), 897-905. https://doi.org/10.1016/j.str.2008.05.001

Hanulová, M., & Weiss, M. (2012). Protein sorting and membrane-mediated interactions. *Biophys Rev*, *4*(2), 117-124. https://doi.org/10.1007/s12551-012-0069-8

Himanen, J. P., Saha, N., & Nikolov, D. B. (2007). Cell-cell signaling via Eph receptors and ephrins. *Curr Opin Cell Biol*, *19*(5), 534-542. https://doi.org/10.1016/j.ceb.2007.08.004

Hite, R. K., Chiu, P. L., Schuller, J. M., & Walz, T. (2015). Effect of lipid head groups on double-layered two-dimensional crystals formed by aquaporin-0. *PLoS One*, *10*(1), e0117371. https://doi.org/10.1371/journal.pone.0117371

Hite, R. K., Li, Z., & Walz, T. (2010). Principles of membrane protein interactions with annular lipids deduced from aquaporin-0 2D crystals. *EMBO J*, *29*(10), 1652-1658. https://doi.org/10.1038/emboj.2010.68

Huang, C. S., Yu, X., Fordstrom, P., Choi, K., Chung, B. C., Roh, S. H., Chiu, W., Zhou, M., Min, X., & Wang, Z. (2020). Cryo-EM structures of NPC1L1 reveal mechanisms of cholesterol transport and ezetimibe inhibition. *Sci Adv*, *6*(25), eabb1989. https://doi.org/10.1126/sciadv.abb1989

Janes, P. W., Ley, S. C., & Magee, A. I. (1999). Aggregation of lipid rafts accompanies signaling via the T cell antigen receptor. *J Cell Biol*, *147*(2), 447-461.

Karnovsky, M. J., Kleinfeld, A. M., Hoover, R. L., & Klausner, R. D. (1982). The concept of lipid domains in membranes. *J Cell Biol*, *94*(1), 1-6.

Kistler, J., & Bullivant, S. (1980). Lens gap junctions and orthogonal arrays are unrelated. *FEBS Lett*, *111*(1), 73-78.

Korade, Z., & Kenworthy, A. K. (2008). Lipid rafts, cholesterol, and the brain. *Neuropharmacology*, *55*(8), 1265-1273. https://doi.org/10.1016/j.neuropharm.2008.02.019

Kumar, V. V. (1991). Complementary molecular shapes and additivity of the packing parameter of lipids. *Proc Natl Acad Sci U S A*, *88*(2), 444-448.

Lafleur, M., Bloom, M., & Cullis, P. R. (1990). Lipid polymorphism and hydrocarbon order. *Biochem Cell Biol*, *68*(1), 1-8.

Lang, T., Bruns, D., Wenzel, D., Riedel, D., Holroyd, P., Thiele, C., & Jahn, R. (2001). SNAREs are concentrated in cholesterol-dependent clusters that define docking and fusion sites for exocytosis. *EMBO J*, *20*(9), 2202-2213. https://doi.org/10.1093/emboj/20.9.2202

Lee, A. G. (2018). A Database of Predicted Binding Sites for Cholesterol on Membrane Proteins, Deep in the Membrane. *Biophys J*, *115*(3), 522-532. https://doi.org/10.1016/j.bpj.2018.06.022

Li, H., & Papadopoulos, V. (1998). Peripheral-type benzodiazepine receptor function in cholesterol transport. Identification of a putative cholesterol recognition/interaction

amino acid sequence and consensus pattern. *Endocrinology*, *139*(12), 4991-4997. https://doi.org/10.1210/endo.139.12.6390

Li, X., Mooney, P., Zheng, S., Booth, C. R., Braunfeld, M. B., Gubbens, S., David, D. A., & Cheng, Y. (2013). Electron counting and beam-induced motion correction enable near-atomic-resolution single-particle cryo-EM. *Nat Methods*, *10*(6), 584-590. https://doi.org/10.1038/nmeth.2472

Lillemeier, B. F., Pfeiffer, J. R., Surviladze, Z., Wilson, B. S., & Davis, M. M. (2006). Plasma membrane-associated proteins are clustered into islands attached to the cytoskeleton. *Proc Natl Acad Sci U S A*, *103*(50), 18992-18997. https://doi.org/10.1073/pnas.0609009103

Lingwood, D., & Simons, K. (2010). Lipid rafts as a membrane-organizing principle. *Science*, *327*(5961), 46-50. https://doi.org/10.1126/science.1174621

Liscum, L., & Munn, N. J. (1999). Intracellular cholesterol transport. *Biochim Biophys Acta*, *1438*(1), 19-37.

Lundbaek, J. A., Andersen, O. S., Werge, T., & Nielsen, C. (2003). Cholesterol-induced protein sorting: an analysis of energetic feasibility. *Biophys J*, *84*(3), 2080-2089. https://doi.org/10.1016/S0006-3495(03)75015-2

Marsh, D. (2010). Liquid-ordered phases induced by cholesterol: a compendium of binary phase diagrams. *Biochim Biophys Acta*, *1798*(3), 688-699. https://doi.org/10.1016/j.bbamem.2009.12.027

Mathiharan, Y. K., Glaaser, I. W., Zhao, Y., Robertson, M. J., Skiniotis, G., & Slesinger, P. A. (2021). Structural insights into GIRK2 channel modulation by cholesterol and PIP. *Cell Rep*, *36*(8), 109619. https://doi.org/10.1016/j.celrep.2021.109619

McCoy, A. J., Grosse-Kunstleve, R. W., Adams, P. D., Winn, M. D., Storoni, L. C., & Read, R. J. (2007). Phaser crystallographic software. *J Appl Crystallogr*, *40*(Pt 4), 658-674. https://doi.org/10.1107/S0021889807021206

McGaughey, G. B., Gagné, M., & Rappé, A. K. (1998). pi-Stacking interactions. Alive and well in proteins. *J Biol Chem*, *273*(25), 15458-15463.

Mejía, R., Gómez-Eichelmann, M. C., & Fernández, M. S. (1999). Fatty acid profile of Escherichia coli during the heat-shock response. *Biochem Mol Biol Int*, *47*(5), 835-844.

Merklinger, E., Schloetel, J. G., Weber, P., Batoulis, H., Holz, S., Karnowski, N., Finke, J., & Lang, T. (2017). The packing density of a supramolecular membrane protein cluster is controlled by cytoplasmic interactions. *Elife*, *6*. https://doi.org/10.7554/eLife.20705

Moriarty, N. W., Grosse-Kunstleve, R. W., & Adams, P. D. (2009). electronic Ligand Builder and Optimization Workbench (eLBOW): a tool for ligand coordinate and restraint generation. *Acta Crystallogr D Biol Crystallogr*, *65*(Pt 10), 1074-1080. https://doi.org/10.1107/S0907444909029436

Mugler, A., Tostevin, F., & ten Wolde, P. R. (2013). Spatial partitioning improves the reliability of biochemical signaling. *Proc Natl Acad Sci U S A*, *110*(15), 5927-5932. https://doi.org/10.1073/pnas.1218301110

Nicolson, G. L. (2014). The Fluid-Mosaic Model of Membrane Structure: still relevant to understanding the structure, function and dynamics of biological membranes after more than 40 years. *Biochim Biophys Acta*, *1838*(6), 1451-1466. https://doi.org/10.1016/j.bbamem.2013.10.019

Nishio, M., Umezawa, Y., Hirota, M., & Takeuchi, Y. (1995). The CH/π interaction: Significance in molecular recognition. *Tetrahedron*, *51*(32), 8665-8701. https://doi.org/https://doi.org/10.1016/0040-4020(94)01066-9

Niu, S. L., & Litman, B. J. (2002). Determination of membrane cholesterol partition coefficient using a lipid vesicle-cyclodextrin binary system: effect of phospholipid acyl chain unsaturation and headgroup composition. *Biophys J*, *83*(6), 3408-3415. https://doi.org/10.1016/S0006-3495(02)75340-X

O'Connor, J. W., & Klauda, J. B. (2011). Lipid membranes with a majority of cholesterol: applications to the ocular lens and aquaporin 0. *J Phys Chem B*, *115*(20), 6455-6464. https://doi.org/10.1021/jp108650u

Orjuela, J. D., Chiu, P.-L., Walz, T., de Groot, B. L., & Aponte-Santamaría, C. stabilizes aquaporin-0 arrays by strengthening the association of adjacent tetramers. *Submitted*.

Pandit, S. A., Khelashvili, G., Jakobsson, E., Grama, A., & Scott, H. L. (2007). Lateral organization in lipid-cholesterol mixed bilayers. *Biophys J*, *92*(2), 440-447. https://doi.org/10.1529/biophysj.106.093864

Pettersen, E. F., Goddard, T. D., Huang, C. C., Couch, G. S., Greenblatt, D. M., Meng, E. C., & Ferrin, T. E. (2004). UCSF Chimera--a visualization system for exploratory research and analysis. *J Comput Chem*, *25*(13), 1605-1612. https://doi.org/10.1002/jcc.20084

Quinn, P. J., & Wolf, C. (2009). The liquid-ordered phase in membranes. *Biochim Biophys Acta*, *1788*(1), 33-46. https://doi.org/10.1016/j.bbamem.2008.08.005

Raguz, M., Mainali, L., Widomska, J., & Subczynski, W. K. (2011). The immiscible cholesterol bilayer domain exists as an integral part of phospholipid bilayer

membranes. *Biochim Biophys Acta*, *1808*(4), 1072-1080. https://doi.org/10.1016/j.bbamem.2010.12.019

Rodal, S. K., Skretting, G., Garred, O., Vilhardt, F., van Deurs, B., & Sandvig, K. (1999). Extraction of cholesterol with methyl-beta-cyclodextrin perturbs formation of clathrin-coated endocytic vesicles. *Mol Biol Cell*, *10*(4), 961-974.

Róg, T., & Pasenkiewicz-Gierula, M. (2006). Cholesterol-sphingomyelin interactions: a molecular dynamics simulation study. *Biophys J*, *91*(10), 3756-3767. https://doi.org/10.1529/biophysj.106.080887

Sarkar, P., & Chattopadhyay, A. (2020). Cholesterol interaction motifs in G protein-coupled receptors: Slippery hot spots? *Wiley Interdiscip Rev Syst Biol Med*, *12*(4), e1481. https://doi.org/10.1002/wsbm.1481

Schenk, A. D., Philippsen, A., Engel, A., & Walz, T. (2013). A pipeline for comprehensive and automated processing of electron diffraction data in IPLT. *J Struct Biol*, *182*(2), 173-185. https://doi.org/10.1016/j.jsb.2013.02.017

Schmidt, U., Guigas, G., & Weiss, M. (2008). Cluster formation of transmembrane proteins due to hydrophobic mismatching. *Phys Rev Lett*, *101*(12), 128104. https://doi.org/10.1103/PhysRevLett.101.128104

Schroeder, F., Jefferson, J. R., Kier, A. B., Knittel, J., Scallen, T. J., Wood, W. G., & Hapala, I. (1991). Membrane cholesterol dynamics: cholesterol domains and kinetic pools. *Proc Soc Exp Biol Med*, *196*(3), 235-252.

Seelig, J. (1977). Deuterium magnetic resonance: theory and application to lipid membranes. *Q Rev Biophys*, *10*(3), 353-418.

Sheets, E. D., Holowka, D., & Baird, B. (1999). Critical role for cholesterol in Lyn-mediated tyrosine phosphorylation of FcepsilonRI and their association with detergent-resistant membranes. *J Cell Biol*, *145*(4), 877-887.

Shinoda, T., Ogawa, H., Cornelius, F., & Toyoshima, C. (2009). Crystal structure of the sodium-potassium pump at 2.4 A resolution. *Nature*, *459*(7245), 446-450. https://doi.org/10.1038/nature07939

Silvius, J. R. (2003). Role of cholesterol in lipid raft formation: lessons from lipid model systems. *Biochim Biophys Acta*, *1610*(2), 174-183.

Simons, K., & Ikonen, E. (1997). Functional rafts in cell membranes. *Nature*, *387*(6633), 569-572. https://doi.org/10.1038/42408

Simons, K., & Toomre, D. (2000). Lipid rafts and signal transduction. *Nat Rev Mol Cell Biol*, *1*(1), 31-39. https://doi.org/10.1038/35036052

Singer, S. J., & Nicolson, G. L. (1972). The fluid mosaic model of the structure of cell membranes. *Science*, *175*(4023), 720-731.

Stier, A., & Sackmann, E. (1973). Spin labels as enzyme substrates. Heterogeneous lipid distribution in liver microsomal membranes. *Biochim Biophys Acta*, *311*(3), 400-408.

Subtil, A., Gaidarov, I., Kobylarz, K., Lampson, M. A., Keen, J. H., & McGraw, T. E. (1999). Acute cholesterol depletion inhibits clathrin-coated pit budding. *Proceedings of the National Academy of Sciences*, *96*(12), 6775-6780. https://doi.org/10.1073/pnas.96.12.6775

Taghon, G. J., Rowe, J. B., Kapolka, N. J., & Isom, D. G. (2021). Predictable cholesterol binding sites in GPCRs lack consensus motifs. *Structure*, *29*(5), 499-506.e493. https://doi.org/10.1016/j.str.2021.01.004

Valpuesta, J. M., Carrascosa, J. L., & Henderson, R. (1994). Analysis of electron microscope images and electron diffraction patterns of thin crystals of phi 29 connectors in ice. *J Mol Biol*, *240*(4), 281-287.

van Meer, G., Voelker, D. R., & Feigenson, G. W. (2008). Membrane lipids: where they are and how they behave. *Nat Rev Mol Cell Biol*, *9*(2), 112-124. https://doi.org/10.1038/nrm2330

Varshney, P., Yadav, V., & Saini, N. (2016). Lipid rafts in immune signalling: current progress and future perspective. *Immunology*, *149*(1), 13-24. https://doi.org/10.1111/imm.12617

Vereb, G., Matkó, J., Vámosi, G., Ibrahim, S. M., Magyar, E., Varga, S., Szöllösi, J., Jenei, A., Gáspár, Jr., R., Waldmann, T. A., & Damjanovich, S. (2000). Cholesterol-dependent clustering of IL-2Rα and its colocalization with HLA and CD48 on T lymphoma cells suggest their functional association with lipid rafts. *Proc Natl Acad Sci U S A*, *97*(11), 6013-6018.

Vereb, G., Szöllosi, J., Matkó, J., Nagy, P., Farkas, T., Vigh, L., Mátyus, L., Waldmann, T. A., & Damjanovich, S. (2003). Dynamic, yet structured: The cell membrane three decades after the Singer-Nicolson model. *Proc Natl Acad Sci U S A*, *100*(14), 8053-8058. https://doi.org/10.1073/pnas.1332550100

Winn, M. D., Ballard, C. C., Cowtan, K. D., Dodson, E. J., Emsley, P., Evans, P. R., Keegan, R. M., Krissinel, E. B., Leslie, A. G. W., McCoy, A., McNicholas, S. J., Murshudov, G. N., Pannu, N. S., Potterton, E. A., Powell, H. R., Read, R. J., Vagin, A., & Wilson, K. S. (2011). Overview of the CCP4 suite and current developments.

Acta Crystallogr D Biol Crystallogr, *67*(Pt 4), 235-242. https://doi.org/10.1107/S0907444910045749

Yeagle, P. L. (1985). Cholesterol and the cell membrane. *Biochim Biophys Acta*, *822*(3-4), 267-287.

Zampighi, G., Simon, S. A., Robertson, J. D., McIntosh, T. J., & Costello, M. J. (1982). On the structural organization of isolated bovine lens fiber junctions. *J Cell Biol*, *93*(1), 175-189.

Zelenka, P. S. (1984). Lens lipids. *Curr Eye Res*, *3*(11), 1337-1359.

Zheng, L., McQuaw, C. M., Ewing, A. G., & Winograd, N. (2007). Sphingomyelin/phosphatidylcholine and cholesterol interactions studied by imaging mass spectrometry. *J Am Chem Soc*, *129*(51), 15730-15731. https://doi.org/10.1021/ja0741675

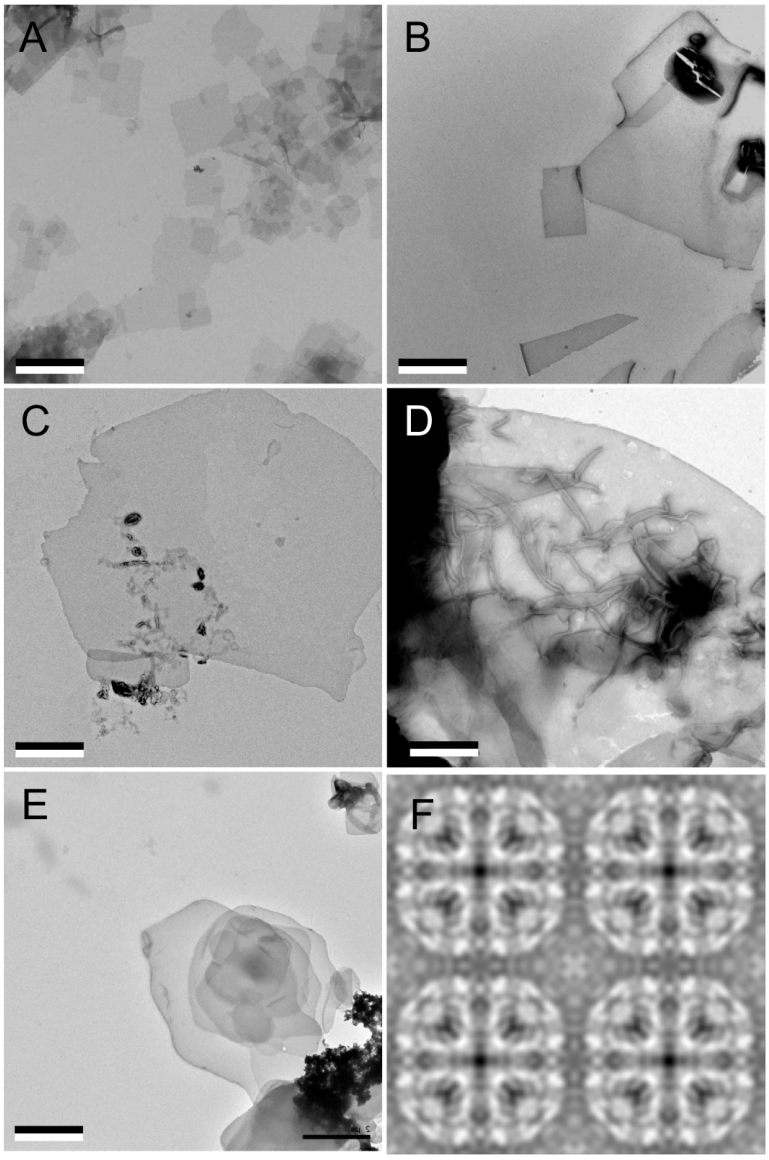

Figure 1. AQP0 forms 2D crystals with all tested sphingomyelin/cholesterol mixtures. (**A-E**) AQP0 purified from sheep lenses was reconstituted with pure sphingomyelin (A), sphingomyelin/cholesterol mixtures at molar ratios of 2:1 (B), 1:2 (C), and 1:4 (D), as well a pure cholesterol (E). AQP0 was reconstituted under all conditions and formed diffracting 2D crystals. The scale bars are 2 μm. (**F**) Projection map of AQP0 reconstituted with pure cholesterol at 3.2 Å resolution. The 2D crystals show *p*422 symmetry and have the typical lattice constants for AQP0 crystals of $a = b = 65.5$ Å, and $\gamma = 90^{o}$. The panel shows two-by-two unit cells. See also Figure 1–figure supplements 1 and 2 and Tables 1 and 2.

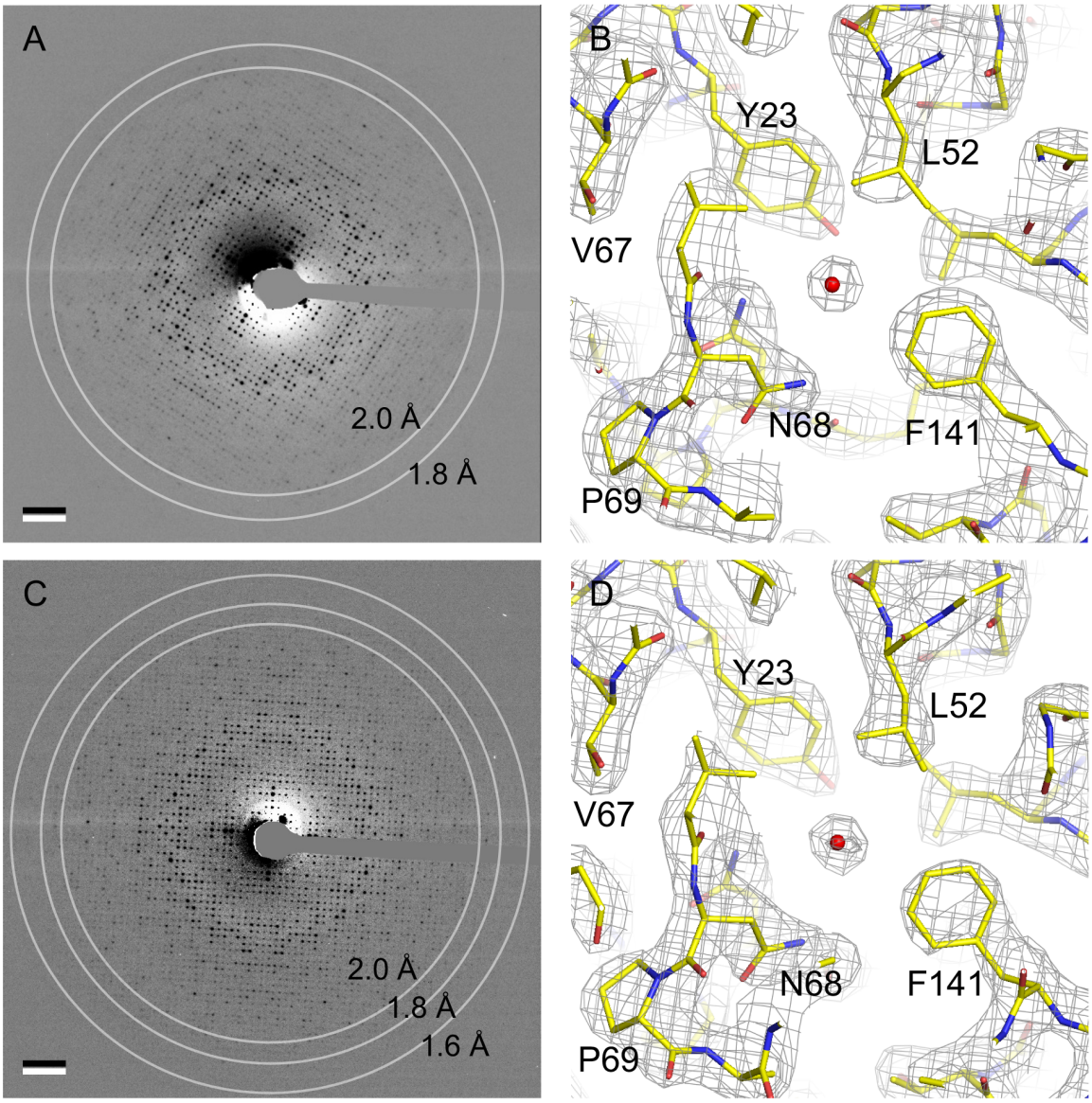

Figure 2. Electron crystallography provides structures of AQP0 in sphingomyelin/ cholesterol bilayers at 2.5-Å resolution. (**A**) Electron diffraction pattern of an untilted AQP0 2D crystal reconstituted at a sphingomyelin:cholesterol ratio of 2:1, showing reflections to ~2 Å resolution. Scale bar indicates $(10\ \text{Å})^{-1}$. (**B**) Density map at 2.5 Å resolution used to build the $AQP0_{2SM:1Chol}$ structure. The 2Fo-Fc map contoured at 1.5σ is shown as gray mesh, the AQP0 model is shown in yellow with oxygen atoms in red and nitrogen atoms in blue. The red sphere represents a water molecule. (**C**) A diffraction pattern of an untilted AQP0 2D crystal reconstituted at a sphingomyelin:cholesterol ratio of 1:2, showing reflections to better than 1.6-Å resolution. Scale bar indicates $(10\ \text{Å})^{-1}$. (**D**) Density map at 2.5-Å resolution used to build the $AQP0_{1SM:2Chol}$ structure. Color code as in (B). See also Figure 2–figure supplement 1.

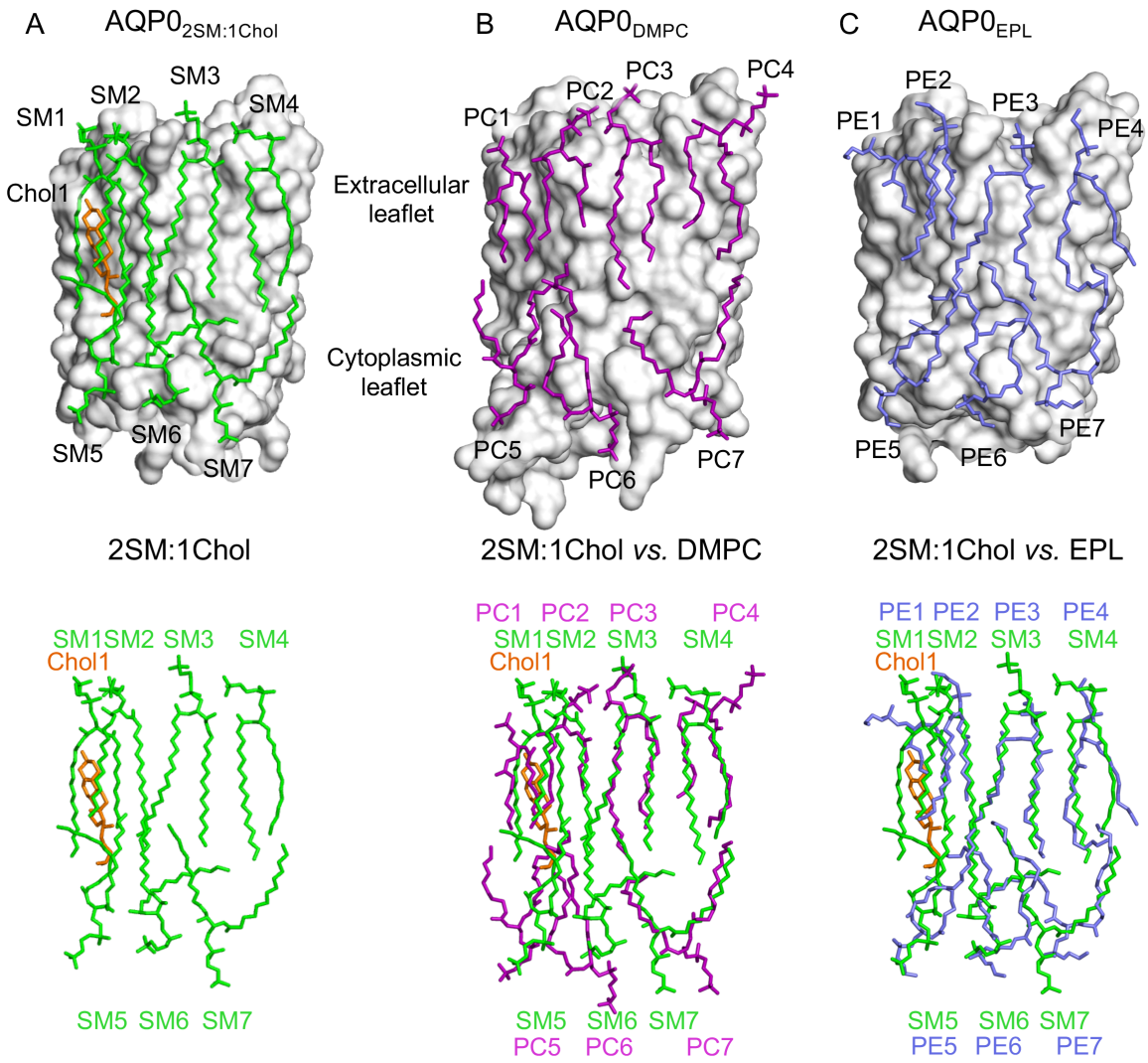

Figure 3. The 2:1 sphingomyelin/cholesterol bilayer surrounding AQP0 is similar to bilayers formed by phosphoglycerolipids. (**A**) The top panel shows the seven sphingomyelins (light green sticks) and one cholesterol (orange sticks) molecules forming the bilayer around an AQP0 subunit (gray surface). The bottom panel shows just the lipid bilayer. (**B**) The top panel shows DMPC lipids (purple sticks) surrounding an AQP0 subunit (Gonen et al., 2005) and the bottom layer shows an overlay of the DMPC bilayer with the 2:1 sphingomyelin/cholesterol bilayer. (**C**) The top panel shows an *E. coli* polar lipids (EPL) bilayer (modeled as PE lipids) (light brown sticks) surrounding an AQP0 subunit (Hite et al., 2010) and the bottom layer shows an overlay of the EPL bilayer with the 2:1 sphingomyelin/cholesterol bilayer. See also Figure 3–figure supplements 1–3 and Table 3.

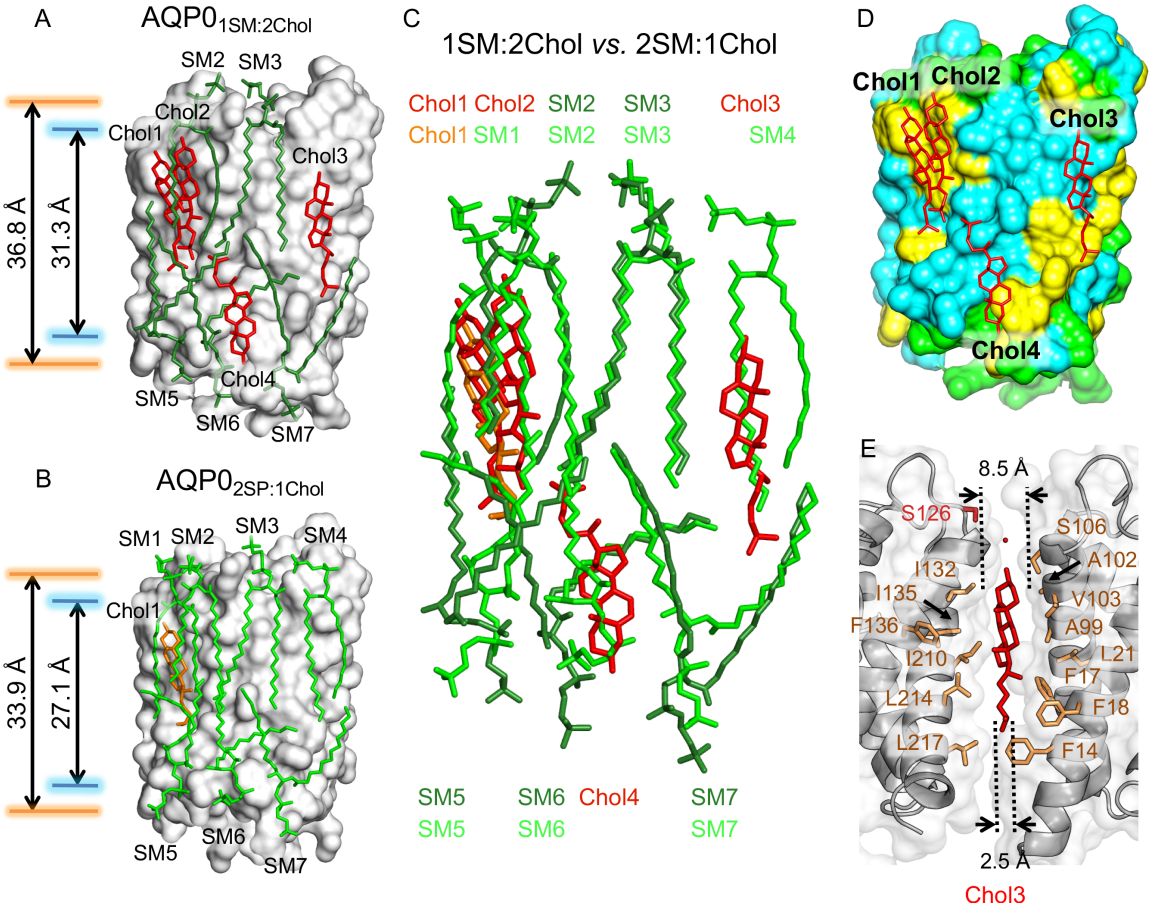

Figure 4. The 1:2 sphingomyelin/cholesterol bilayer surrounding AQP0 and comparison with the 2:1 sphingomyelin/cholesterol bilayer. (**A**) The five sphingomyelins (dark green sticks) and four cholesterol (red sticks) molecules surrounding an AQP0 subunit (gray surface). The arrows between the orange and blue lines indicate the average distances between the phosphor atoms of the phosphodiester groups and the nitrogen atoms of the amide groups in the two leaflets, respectively. (**B**) The $AQP0_{2SM:1Chol}$ structure shown for comparison with the $AQP0_{1SM:2Chol}$ structure in (A). Arrows as in (A). (**C**) Overlay of the lipid bilayers in the $AQP0_{2SM:1Chol}$ and $AQP0_{1SM:2Chol}$ structures. (**D**) Location of the four cholesterols (red sticks) in the $AQP0_{1SM:2Chol}$ structure with respect to AQP0 surface characteristics. Color coding: yellow, aromatic residues; cyan, hydrophobic residues; and light green, polar and charged residues. (**E**) Position of cholesterol Chol3 (red sticks) in the $AQP0_{1SM:2Chol}$ structure and its interaction with residues of two adjacent AQP0 tetramers (brown sticks). See also Figure 4–figure supplements 1–2 and Table 3.

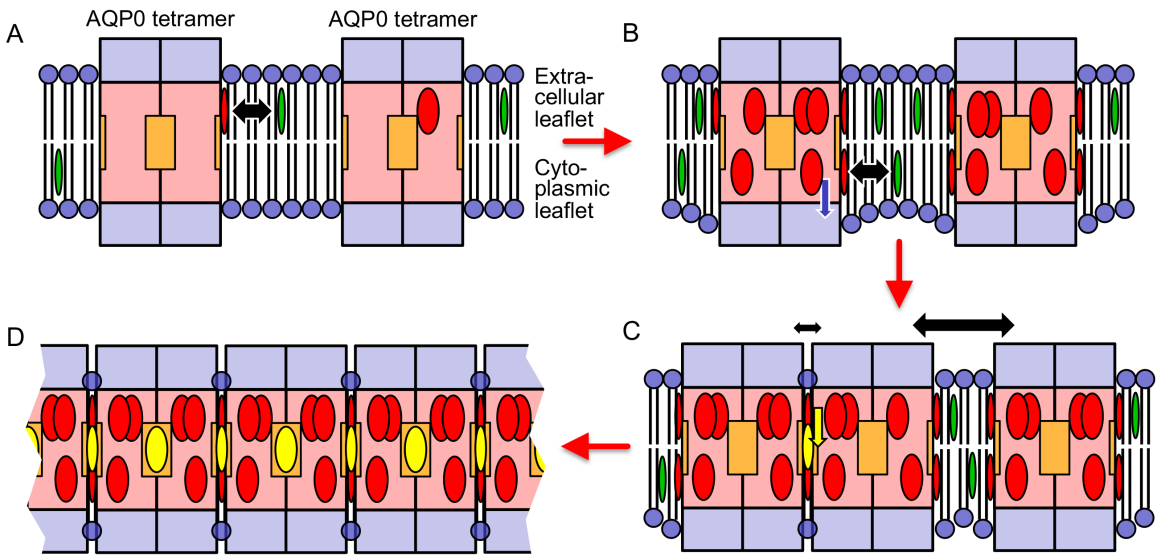

Figure 5. Proposed model for how an increasing cholesterol concentration drives AQP0 2D array formation in the native lens membrane. (**A**) At a low cholesterol concentration, AQP0 tetramers are mostly surrounded by phospholipids and sphingomyelin. Free cholesterol in the membrane (green ovals) only associates with the highest affinity cholesterol-binding sites. Cholesterols occupying these peripheral binding sites are shown as red ovals and the black double-headed arrow indicates the transient nature of this interaction. The deep cholesterol-binding sites (orange squares) are not occupied. (**B**) With increasing cholesterol concentration, more cholesterols associate with the AQP0 surface. These cholesterols cause the interacting lipids in the cytoplasmic leaflet to move out from the bilayer center (blue arrow), resulting in the annular lipid shell that has a bigger hydrophobic thickness than the surrounding membrane, creating a hydrophobic mismatch that results in membrane deformation. (**C**) To minimize hydrophobic mismatch, AQP0 tetramers cluster. Cholesterol in between adjacent tetramers can move into the deep binding sites (yellow arrow) and cholesterol occupying deep binding sites (yellow ovals) act as glue that increases that association of the adjacent tetramers (indicated by the small double-headed black arrow) as compared to adjacent tetramers that do not sandwich a deep-binding cholesterol (indicated by the large double-headed black arrow). Clustering of proteins to minimize hydrophobic mismatch and stabilization by deep cholesterol-mediated protein–protein interactions may be the basis for the formation of transient lipid rafts. (**D**) Each AQP0 tetramer has four deep cholesterol-binding sites. As a result of the avidity effect, AQP0 can form large and stable 2D arrays.